Simultaneous inversion for source field and mantle electrical conductivity using the variable projection approach

Jingtao Min [1] Alexander Grayver [2,1]

[1]Institut für Geophysik, ETH Zürich

[2]Institut für Geophysik und Meteorologie, Universität zu Köln

July 13, 2023

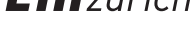

Contents

Contents

Electric current systems of the Earth

- Magnetosphere
- Ionosphere
- Tidal currents
- Mantle currents
- Core currents

- Inducing current $\mathbf{j}$
- Induced current $\mathbf{j}^{(1)}$

Pre-Maxwell's Equations

$$\nabla \times \mathbf{E} = -i\omega \mathbf{B},$$
$$\frac{1}{\mu_0} \nabla \times \mathbf{B} = \mathbf{j} + \mathbf{j}^{(1)} = \mathbf{j} + \sigma \mathbf{E}$$

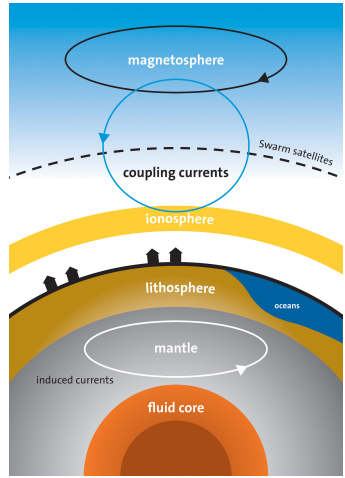

Figure: Current systems of Earth (src: DTU/ESA)

Electromagnetic induction problem in a nutshell

Forward modelling: electromagnetic induction modelling

Frequency domain: $\mathbf{B}(\mathbf{r}, \omega; \sigma) = \int_{\Omega} \mathbf{G}(\mathbf{r}, \mathbf{r}', \omega; \sigma) \cdot \mathbf{j}(\mathbf{r}', \omega)\, d\mathbf{r}'$

Time domain: $\mathbf{B}(\mathbf{r}, t; \sigma) = \int_{\mathbb{R}} \int_{\Omega} \mathbf{G}(\mathbf{r}, \mathbf{r}', t - t'; \sigma) \cdot \mathbf{j}(\mathbf{r}', t')\, d\mathbf{r}'\, dt'$

Electrical conductivity σ
Ionospheric/magnetospheric electric current $\mathbf{j}$

$(\sigma, \mathbf{j}) \underset{\text{inverse}}{\overset{\text{forward}}{\rightleftharpoons}} \mathbf{B}$

Observable magnetic field $\mathbf{B}$ (or electric field)

Inverse problem: electromagnetic induction sounding
Retrieve the model by minimizing the data misfit and solving the optimization problem:

$$\min_{\sigma, \mathbf{j}} L(\mathbf{B}^{\text{mod}}(\sigma, \mathbf{j}), \mathbf{B}^{\text{obs}})$$

Electromagnetic induction problem in a nutshell

Forward modelling: electromagnetic induction modelling
A unified algebraic form:

$$\mathbf{d} = \mathbf{F}(\sigma)\mathbf{c}$$

Electrical conductivity σ
Source current parameter $\mathbf{c}$

$$(\sigma, \mathbf{c}) \underset{\text{inverse}}{\overset{\text{forward}}{\rightleftharpoons}} \mathbf{d}$$

Observables $\mathbf{d}$

Inverse problem: electromagnetic induction sounding
Optimization problem posed as a Separable Nonlinear Least Squares (SNLS):

$$\min_{\sigma,\mathbf{c}} \frac{1}{2}\|\mathbf{r}(\sigma,\mathbf{c})\|^2 + \frac{\lambda}{2}\|\mathbf{\Gamma}\sigma\|_2^2, \qquad \mathbf{r} = \mathbf{d}^{\text{obs}} - \mathbf{F}(\sigma)\mathbf{c}$$

Highlight

- An efficient way to tackle the joint model space inversion in EM induction sounding
- Simultaneous estimation of σ and $\mathbf{c}$

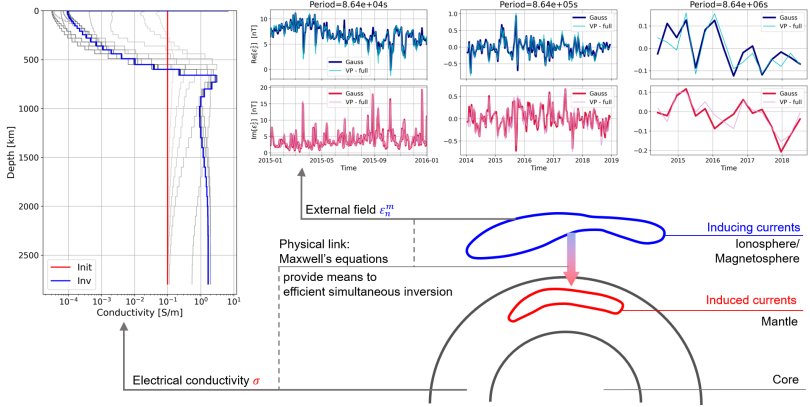

Contents

Approaches to the joint model space

Inverse problem in EM induction sounding

$$\min_{\sigma,\mathbf{c}} \frac{1}{2}\|\mathbf{r}(\sigma,\mathbf{c})\|^2 + \frac{\lambda}{2}\|\mathbf{\Gamma}\sigma\|_2^2, \qquad \mathbf{r} = \mathbf{d}^{\text{obs}} - \mathbf{F}(\sigma)\mathbf{c}$$

Why is it challenging?

Joint model space of σ and $\mathbf{c}$ is very high-dimensional

How to deal with it?

- Variable projection method (VP) for Separable Nonlinear Least Squares (SNLS)
- Alternating approaches

Variable projection

Inverse problem in EM induction sounding

$$\min_{\sigma,\mathbf{c}} \frac{1}{2}\|\mathbf{r}(\sigma,\mathbf{c})\|^2 + \frac{\lambda}{2}\|\mathbf{\Gamma}\sigma\|_2^2, \qquad \mathbf{r} = \mathbf{d}^{\text{obs}} - \mathbf{F}(\sigma)\mathbf{c}$$

When given σ, the best fitting $\mathbf{c}$ can be easily found via linear least squares!

$$\hat{\mathbf{c}}(\sigma) = \mathbf{F}^{\dagger}(\sigma)\mathbf{d} = -\mathbf{J}_c^{\dagger}(\sigma)\mathbf{d}$$

Formulating $\mathbf{c}$ as a function of σ, the optimization can be conducted solely in σ instead of in the joint model space

EM sounding problem viewed from variable projection (VP)

$$\min_{\sigma} \frac{1}{2}\|\mathbf{r}(\sigma,\hat{\mathbf{c}}(\sigma))\|_2^2 + \frac{\lambda}{2}\|\mathbf{\Gamma}\sigma\|_2^2$$

Variable Projection: toy example explained

- Fitting a wavelet signal

$$y(t) = 2c\alpha(1 - 2\alpha t^2)\exp\left(-\alpha t^2\right)$$

- SNLS problem

$$\min_{\alpha,c} \frac{1}{2}\|\mathbf{y} - \boldsymbol{\phi}(\alpha)c\|_2^2$$

$\boldsymbol{\phi} \in \mathbb{R}^n$, and each element is given by

$$\phi(t_i;\alpha) = 2\alpha(1 - 2\alpha t_i^2)\exp\left(-\alpha t_i^2\right)$$

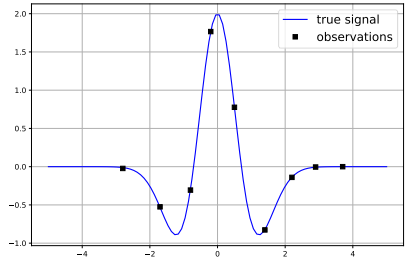

Figure: Data and target signal of fitting

Variable Projection: toy example explained

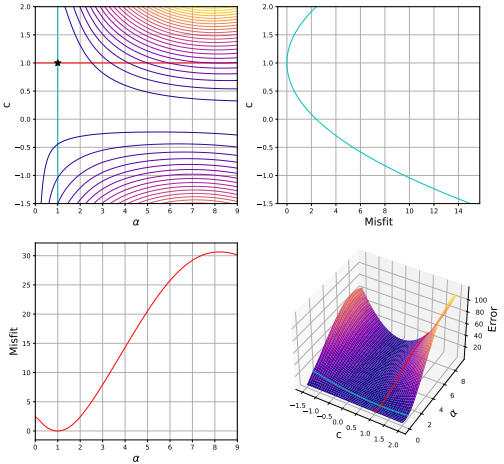

Figure: Topography of the objective function

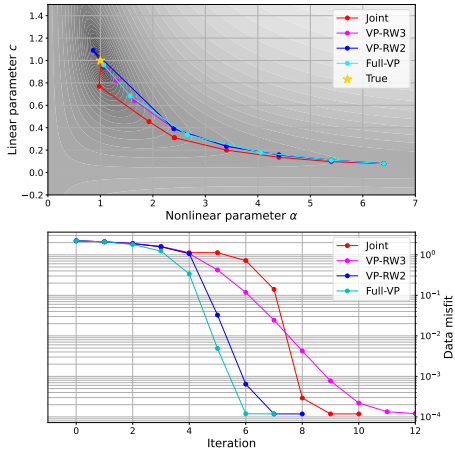

Figure: Iteration trajectory of differenet methods

Alternating approaches

- Alternate between σ updates and $\mathbf{c}$ regressions
- Prototype implementation by Koch and Kuvshinov 2013
- "Linear valley" assumption

(a) Valtellina, N Italy (Swisstopo)

(b) Aletsch glacier, S Switzerland (Swisstopo)

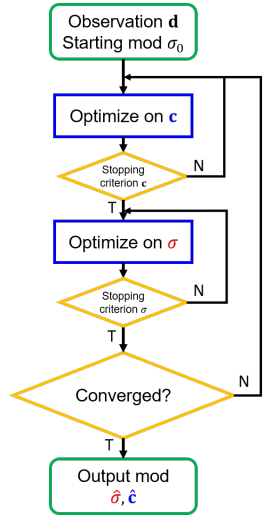

Model parameterization and forward modelling

- Assuming: magnetic field is potential

$$\mathbf{B} = -\nabla V$$

- Spherical harmonic (SH) representation of the potential field

$$V = \sum_{n,m} \left[\varepsilon_n^m \left(\frac{r}{a} \right)^n + \iota_n^m \left(\frac{r}{a} \right)^{-(n+1)} \right] Y_n^m(\theta, \varphi)$$

- Assuming: 1-D structure / radial symmetry

$$\iota_n^m(\omega; \sigma) = Q_n(\omega; \sigma)\, \varepsilon_n^m(\omega)$$

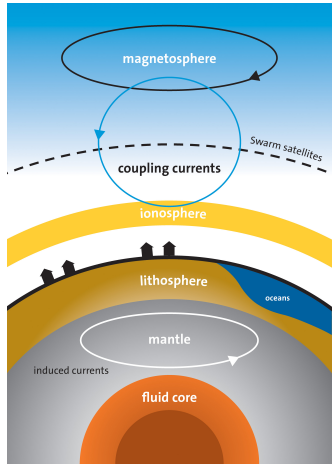

Contents

Model recovery

Methods tested on a synthetic dataset (where σ and $\mathbf{c}$ are known) against conventional method.

For VP / alternating approaches with frequent linear regression (e.g. Alt-Fibonacci):

- ✓ 1-D conductivity recovery
- ✓✓ inducing field spectrum, all modes and frequency bands
- Results comparable to conventional method

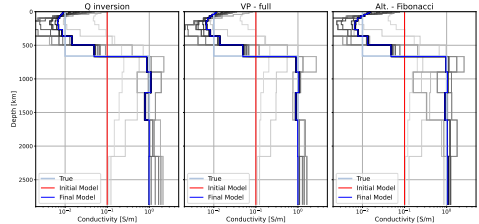

(a) Comparison of recovered mantle conductivity models

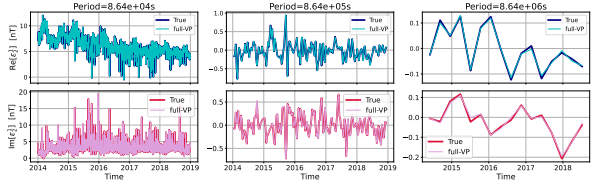

(b) Source field recovery (mode ε_2^1) for VP

Source field update in alternating approaches

- Convergence senstive to update frequency of $\mathbf{c}$
- $\hat{\sigma}$ sensitive to $\hat{\mathbf{c}}$

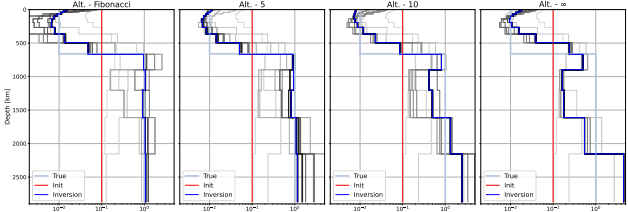

Figure: Conductivity profile recovery for alternating approaches

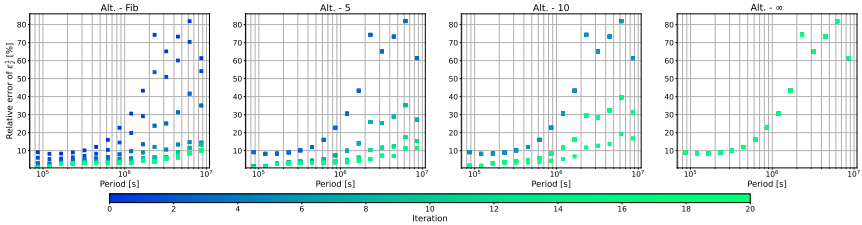

Figure: Relative errors for mode ε_2^1

Source estimation: does conductivity matter?

Simplistic mantle conductivity models are sometimes used to account for induction when estimating the source.

How biased will the source estimate be?

Test the estimates source field assuming three conductivity models:

- VP-inverted conductivity model ("inv")
- Initial uniform conductivity ("init")
- Perfect insulator-conductor model ("bilayer")

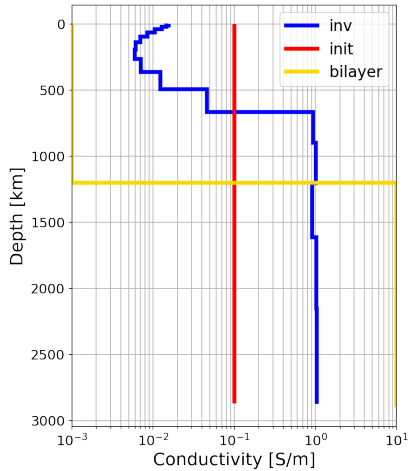

Figure: Inverted and simplistic conductivity models

Source estimation: does conductivity matter?

How biased will the source estimate be?

- ε_1^0: $5 \sim 20\%$ error for simplistic σ models, $< 1.4\%$ for inverted σ model;
- ε_2^1: $10 \sim 80\%$ error for simplistic σ models, $1 \sim 10\%$ for inverted σ model.

$\Longrightarrow$ Overly simplistic models yield significantly higher errors in external field estimates!

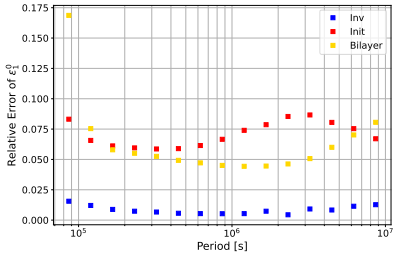

(a) Errors in source field, mode ε_1^0

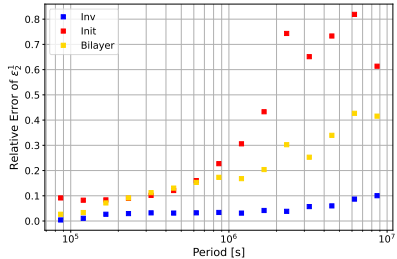

(b) Errors in source field, mode ε_2^1

Source estimation: better conditioned in VP/Alt

Accounting for the induced field by modelling drastically improves the conditioning of the source estimation problem (hence, better separability and resolution).

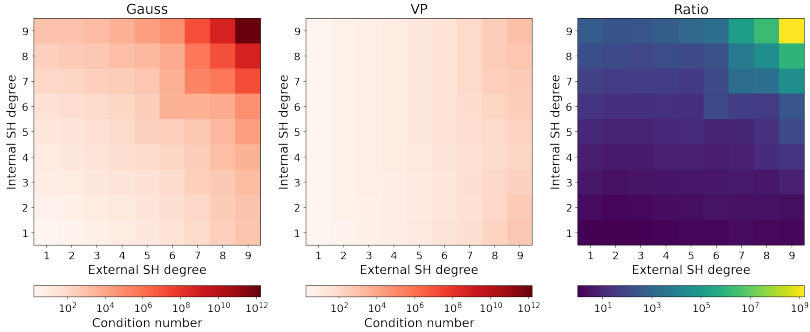

Figure: Condition number of the linear operator in Gauss method, VP, and their ratios

Contents

Real data inversion

The same method is then applied to time series of magnetic field observed at ground observatories (2014-2018).
The source field during this period and the conductivity profile are co-estimated.

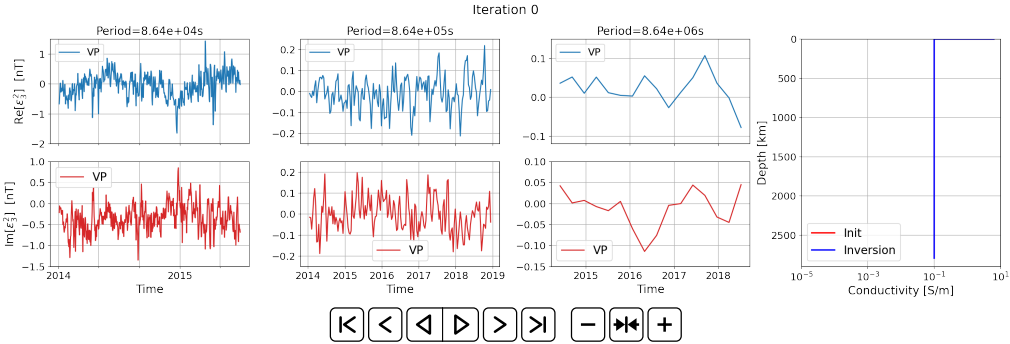

Contents

Summary

- Simultaneous estimation of ionos-/magnetospheric source and mantle conductivity;
- First application of Variable Projection to EM induction sounding;
- Non-trivial correlations between source and conductivity;
- Tested on real data, obtained source field 2014-2018 + 1-D conductivity profile

For details, see our recently published paper in **Earth, Planets and Space**: *Simultaneous inversion for source field and mantle electrical conductivity using the variable projection approach*.

No "best of one world" without "best of both worlds"

Summary

What is next? Framework of variable projection and alternating approaches enables...

- incorporation of prior knowledge on source structure
- incorporation of data from multiple sources (e.g. ground + satellites)
- integration with core-field models (CI, CHAOS)
- new generation of self-consistent external current and mantle conductivity models

Figure: ESA Swarm satellites (image from ESA Earth Online - Swarm Mission)

References I

Aravkin, Aleksandr Y and Tristan van Leeuwen (Oct. 2012). "Estimating nuisance parameters in inverse problems". In: *Inverse Problems* 28.11, p. 115016. DOI: 10.1088/0266-5611/28/11/115016. URL: https://doi.org/10.1088/0266-5611/28/11/115016.

Golub, G. H. and V. Pereyra (1973). "The Differentiation of Pseudo-inverses and Nonlinear Least Square Problems Whose Variables Separate". In: *SIAM Journal of Numerical Analysis* 10 (2), pp. 413–432. DOI: 10.1137/0710036. URL: https://doi.org/10.1137/0710036.

Hansen, Per Christian and Dianne Prost O'Leary (Nov. 1993). "The Use of the L-Curve in the Regularization of Discrete Ill-Posed Problems". In: *SIAM Journal on Scientific Computing* 14 (6), pp. 1487–1503. ISSN: 1064-8275. DOI: 10.1137/0914086. URL: https://doi.org/10.1137/0914086.

Koch, Stephan and Alexey Kuvshinov (July 2013). "Global 3-D EM inversion of Sq variations based on simultaneous source and conductivity determination: concept validation and resolution studies". In: *Geophysical Journal International* 195.1, pp. 98–116. ISSN: 0956-540X. DOI: 10.1093/gji/ggt227. URL: https://doi.org/10.1093/gji/ggt227.

References II

Ruhe, Axel and Per Åke Wedin (Aug. 1980). "Algorithms for Separable Nonlinear Least Squares Problems". In: *SIAM Review* 22 (3), pp. 318–337. ISSN: 0036-1445. DOI: 10.1137/1022057. URL: https://doi.org/10.1137/1022057.

Contents

Synthetic data generation

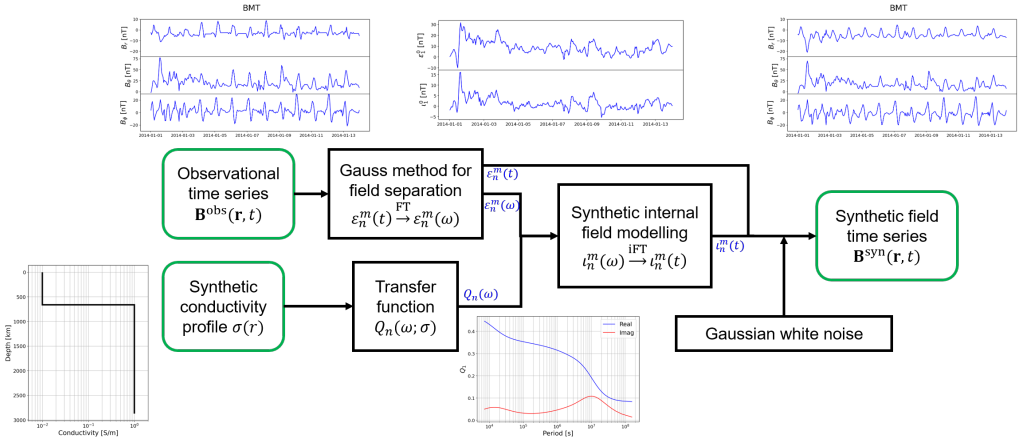

Figure: Workflow of synthetic data generation

Data processing

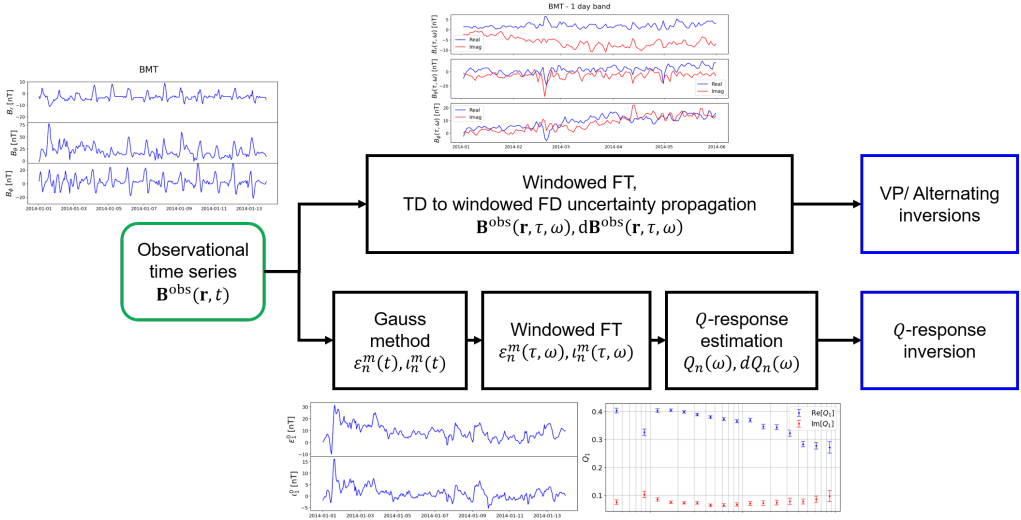

Figure: Workflow of real data processing

Uncertainty estimation

Time-domain noise can propagate into the frequency domain.
Windowed Fourier Transform of a time series $x(t)$ takes the form

$$X(\tau,\omega) = \mathscr{F}_{\tau,\omega}\left[x(t)\right] = \frac{1}{\sum_k w_k} \sum_{k\in\{k_\tau\}} w_k x(t_k)\, e^{-i\omega t_k}$$

Assuming the noise $x'(t)$ is a white noise, i.e.

- are i.i.d. random variables at each time point,
- zero-mean, with standard deviation s,

the uncertainty in the windowed spectrum

$$\mathrm{Var}[X'(\tau,\omega)] = \frac{\sum_k w_k^2}{\left(\sum_k w_k\right)^2} s^2 \sim \frac{s^2}{N}$$

Uncertainty estimation

Time-domain noise can propagate into the frequency domain.

$$\mathbb{E}\left[|X'(\tau,\omega)|^2\right] = \mathbb{E}\left[\frac{1}{\left(\sum_k w_k\right)^2}\sum_{k\in\{k_\tau\}}\sum_{l\in\{l_\tau\}} w_k w_l \overline{x'(t_k)}x'(t_l)e^{i\omega(t_k-t_l)}\right]$$

$$= \frac{1}{\left(\sum_k w_k\right)^2}\sum_{k\in\{k_\tau\}}\sum_{l\in\{l_\tau\}} w_k w_l \,\mathbb{E}\left[\overline{x'(t_k)}x'(t_l)\right] e^{i\omega(t_k-t_l)}$$

$$= \frac{1}{\left(\sum_k w_k\right)^2}\sum_{k\in\{k_\tau\}}\sum_{l\in\{l_\tau\}} w_k w_l \left(s^2\delta_{kl}\right) e^{i\omega(t_k-t_l)} = \frac{\sum_k w_k^2}{\left(\sum_k w_k\right)^2}s^2$$

Uncertainty estimation

In practice, however, the uncertainty has to be water-leveled

$$\epsilon = \sqrt{\epsilon^2_{\text{propagated}} + \epsilon^2_0} = \sqrt{\frac{\sum_k w_k^2}{\left(\sum_k w_k\right)^2} s^2 + \epsilon^2_0}$$

The reason for that is the spectral leakage leads to an extra error that does not scale in the same way as uncertainty propagated from time domain.

Imperfect nature of windowed-Fourier-domain modelling

Windowed spectrum in terms of complete spectrum

$$X(\tau,\omega) = \frac{1}{\sum_k w_k} \sum_{k\in\{k_\tau\}} w_{k-k_{\tau 0}}\, x(t_k)\, e^{-i\omega(t_k - t_{k_{\tau 0}})}$$

$$= \frac{1}{\sqrt{N}} \sum_{q=0}^{N-1} X(\omega_q) \left[\frac{1}{\sum_k w_k} \sum_{p=0}^{K_\tau - 1} w_p\, e^{i(\omega_q-\omega)t_p} \right] e^{i\omega_q t_{k_{\tau 0}}}$$

$$X(\tau,\omega) = \frac{1}{\sqrt{N}} \sum_{q=0}^{N-1} X(\omega_q)\, \widetilde{W}(\omega-\omega_q)\, e^{i\omega_q t_{k_{\tau 0}}}$$

where $\widetilde{W}(\omega) = \frac{1}{\sum_{p=0}^{K_\tau-1} w_p} \sum_{p=0}^{K_\tau-1} w_p\, e^{-i\omega t_p}$ is the spectrum of the window function.

Imperfect nature of windowed-Fourier-domain modelling

Windowed spectra of $x(t)$ and $y(t)$, where $X(\omega) = H(\omega)\, Y(\omega)$

$$X(\tau, \omega) = \frac{1}{\sqrt{N}} \sum_{q=0}^{N-1} X(\omega_q)\ \widetilde{W}(\omega - \omega_q)\ e^{i\omega_q t_{k_\tau 0}}$$

$$Y(\tau, \omega) = \frac{1}{\sqrt{N}} \sum_{q=0}^{N-1} H(\omega_q)\, X(\omega_q)\ \widetilde{W}(\omega - \omega_q)\ e^{i\omega_q t k_{\tau 0}}$$

$\Longrightarrow$ in general the following is NOT exactly satisfied

$$Y(\tau, \omega) = H(\omega) X(\tau, \omega)$$

Inversion in the joint model space

Joint model space, $\mathbf{m} = \begin{bmatrix} \sigma \\ \mathbf{c} \end{bmatrix} \in \mathbb{C}^{M_\sigma + M_c}$

Data residual $\mathbf{r}(\mathbf{m}) = r(\sigma, \mathbf{c})$, its Jacobian $\mathbf{J} = \frac{\partial \mathbf{r}}{\partial(\sigma, \mathbf{c})} = \begin{bmatrix} \mathbf{J}_\sigma & \mathbf{J}_c \end{bmatrix} \in \mathbb{C}^{N \times (M_\sigma + M_c)}$.
Gauss-Newton algorithm:

$$\begin{bmatrix} \mathbf{J}_\sigma^H \mathbf{J}_\sigma + \lambda \mathbf{\Gamma}^T \mathbf{\Gamma} & \mathbf{J}_\sigma^H \mathbf{J}_c \\ \mathbf{J}_c^H \mathbf{J}_\sigma & \mathbf{J}_c^H \mathbf{J}_c \end{bmatrix} \begin{bmatrix} \Delta\sigma \\ \Delta\mathbf{c} \end{bmatrix} = - \begin{bmatrix} \mathbf{J}_\sigma^H \mathbf{r}_w \\ \mathbf{J}_c^H \mathbf{r}_w \end{bmatrix}$$

Dimensionality: solve an augmented system in the $(M_\sigma + M_c)$ dimensional space.
Nonlinearity: both σ and $\mathbf{c}$ are updated in a fully non-linear fashion.

Variable projection

Non-trivial bit: calculation of Fréchet derivatives:

$$\mathbf{J}(\sigma, \hat{\mathbf{c}}(\sigma)) = \mathrm{D}\mathbf{r} = \mathbf{J}_\sigma + \mathbf{J}_c \, \mathrm{D}\hat{\mathbf{c}} = \mathbf{J}_\sigma - \mathbf{J}_c \, \mathrm{D}\mathbf{J}_c^\dagger \, \mathbf{d}_w$$

Fortunately, close-form formula exists (Golub and Pereyra 1973):

Decomposition of the Jacobian

$$\mathbf{J}(\sigma, \hat{\mathbf{c}}(\sigma)) = \mathbf{J}_\sigma - \mathbf{J}_c \mathbf{J}_c^\dagger \mathbf{J}_\sigma - \left(\mathbf{J}_c^\dagger\right)^H (\mathrm{D}\mathbf{J}_c)^H \mathbf{r}_w$$

Variants of Variable Projection

Three variants of variable projection

- Original formulation (VP-full) developed following Golub and Pereyra 1973;
- Second and third algorithms (RW2/RW3), proposed by Ruhe and Wedin 1980;
- Linear constraint (feedback of the linear variable) present in VP-full and VP-RW2, but absent in VP-RW3;

VP - full

$$\begin{aligned}\mathbf{J} &= \mathbf{J}_\sigma - \mathbf{J}_c\mathbf{J}_c^\dagger\mathbf{J}_\sigma - \left(\mathbf{P}^\perp_{\mathbf{J}_c}\mathrm{D}\mathbf{J}_c\mathbf{J}_c^\dagger\right)^H\mathbf{d}_w \\ &= -\mathbf{P}^\perp_{\mathbf{F}_w}\,\mathrm{D}\mathbf{F}_w\,\mathbf{F}_w^\dagger\mathbf{d}_w - (\mathbf{P}^\perp_{\mathbf{F}_w}\,\mathrm{D}\mathbf{F}_w\,\mathbf{F}_w^\dagger)^H\mathbf{d}_w\end{aligned}$$

VP - RW2

$$\mathbf{J} = \mathbf{P}^\perp_{\mathbf{J}_\sigma}\mathbf{J}_\sigma = -\mathbf{P}^\perp_{\mathbf{F}_w}\,\mathrm{D}\mathbf{F}_w\,\mathbf{F}_w^\dagger\mathbf{d}_w$$

VP - RW3

$$\mathbf{J} = \mathbf{J}_\sigma = -\,\mathrm{D}\mathbf{F}_w\,\mathbf{F}_w^\dagger\mathbf{d}_w$$

Inversion schemes tested

Variable Projection

- The full VP
- VP-RW2
- VP-RW3 (no implicit feedback of $\mathbf{c}$)

Alternating approach

- Update $\mathbf{c}$ at iterations following Fibonacci sequence (Alt-Fib)
- Update $\mathbf{c}$ every 5 iters (Alt-5)
- Update $\mathbf{c}$ every 10 iters (Alt-10)
- $\mathbf{c}$ estimated only once at the beginning (Alt-∞)

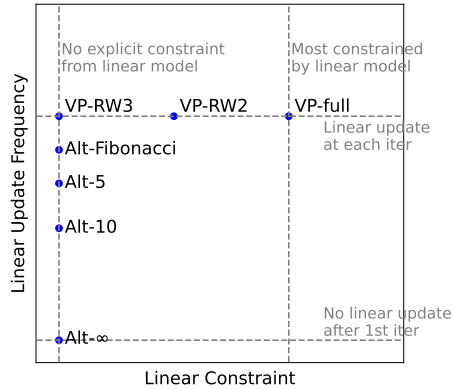

Figure: Schematic plot of inversion schemes

Choice of regularizations

L-curves (Hansen and O'Leary 1993)

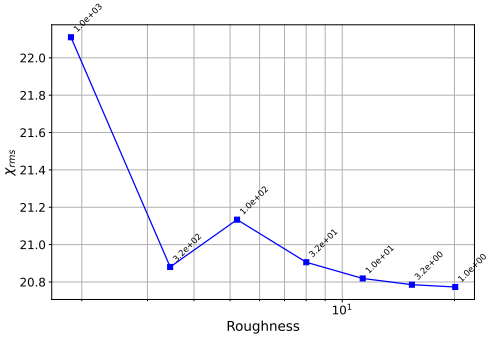

(a) L-curve for Q-response inversion

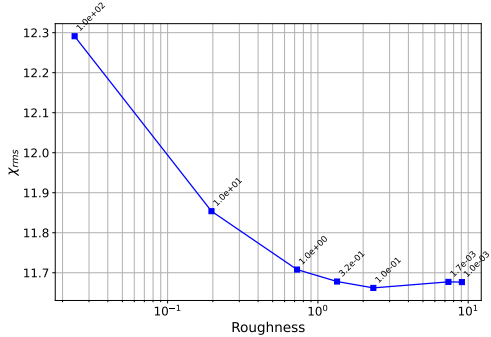

(b) L-curve for VP inversion

VP and Joint model inversion

Superiority of VP-RW2

When starting from $(\sigma, \hat{\mathbf{c}} = -\mathbf{J}_c^{\dagger}\mathbf{d}_w)$ and using Gauss-Newton algorithm, VP-RW2 is guaranteed to propose models with lower misfits than joint model space inversion.

Model update on σ proposed by Gauss-Newton algorithm in joint model space inversion

$$\left[\mathrm{Re}\left[\mathbf{J}_\sigma^H \mathbf{P}_{\mathbf{J}_c}^{\perp} \mathbf{J}_\sigma\right] + \lambda \Gamma^T \Gamma\right] \Delta\sigma = -\mathrm{Re}\left[\mathbf{J}_\sigma^H \mathbf{P}_{\mathbf{J}_c}^{\perp} \mathbf{r}_w\right]$$

Updates using VP variants

$$\left[\mathrm{Re}\left[\mathbf{J}_\sigma^H \mathbf{P}_{\mathbf{J}_c}^{\perp} \mathbf{J}_\sigma + \mathbf{r}_w^H \mathsf{D}\mathbf{J}_c \left(\mathbf{J}_c^H \mathbf{J}_c\right)^{-1} \mathsf{D}\mathbf{J}_c^H \mathbf{r}_w\right] + \lambda \mathbf{\Gamma}^T \mathbf{\Gamma}\right] \Delta\sigma = -\mathrm{Re}\left[\mathbf{J}_\sigma^H \mathbf{r}_w\right] \quad (\mathrm{VP-full})$$

$$\left[\mathrm{Re}\left[\mathbf{J}_\sigma^H \mathbf{P}_{\mathbf{J}_c}^{\perp} \mathbf{J}_\sigma\right] + \lambda \mathbf{\Gamma}^T \mathbf{\Gamma}\right] \Delta\sigma = -\mathrm{Re}\left[\mathbf{J}_\sigma^H \mathbf{r}_w\right] \quad (\mathrm{VP-RW2})$$

$$\left[\mathrm{Re}\left[\mathbf{J}_\sigma^H \mathbf{J}_\sigma\right] + \lambda \mathbf{\Gamma}^T \mathbf{\Gamma}\right] \Delta\sigma = -\mathrm{Re}\left[\mathbf{J}_\sigma^H \mathbf{r}_w\right] \quad (\mathrm{VP-RW3})$$

Gradient-based VP

Regardless of the choice of approximations (VP-full, VP-RW2 or RW3)

$$\mathrm{grad}\chi^2 = \mathrm{D}\chi^2 = \mathrm{Re}\left[\mathbf{J}^H\mathbf{r}_w\right] = -\mathrm{Re}\left[\left(\mathrm{D}\mathbf{J}_c\,\mathbf{J}_c^{\dagger}\mathbf{d}_w\right)^H\mathbf{P}_{\mathbf{J}_c}^{\perp}\mathbf{d}_w\right] = \mathrm{Re}\left[\mathbf{J}_\sigma^H\mathbf{r}_w\right]$$

Therefore when using gradient-based optimizations, the implicit feedback of the inducing source estimate will not play a role.

In fact, consider a general objective function $g(\sigma, c)$, let $\hat{c}(\sigma) = \arg\min_c g(\sigma, c)$ and $\tilde{g}(\sigma) = g(\sigma, \hat{c}(\sigma))$, we have

$$\nabla_\sigma \tilde{g}(\sigma) = \nabla_\sigma g(\sigma, c)$$

i.e. the gradient is also equal to the explicit gradient (Aravkin and Leeuwen 2012).

Contents

Data

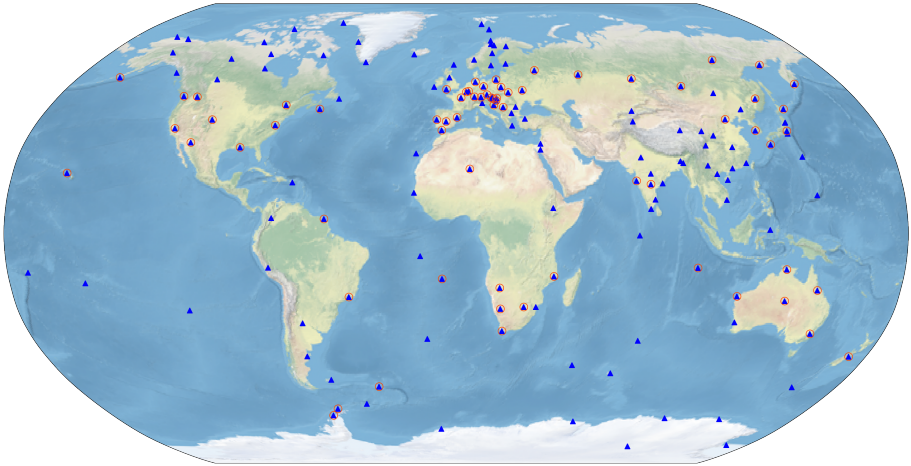

Figure: Observatories

Inducing field estimates

For selected "energetic" modes, VP produces source estimates coherent with Gauss method:

- First zonal harmonic ε_1^0, > 1d
- ε_2^1, diurnal band (≈ 1d)
- ε_3^2, semi-diurnal ($T \approx 12$hr)

Other modes: correlated trends + difference in amplitudes.

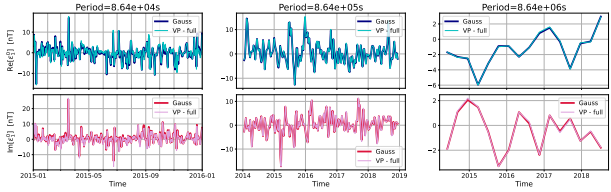

(a) Windowed spectrum of ε_1^0, estimates using Gauss method and VP

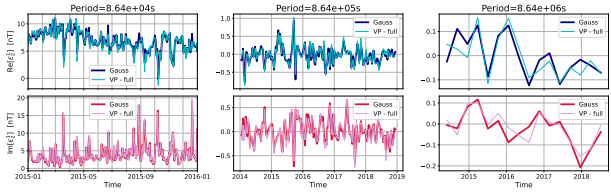

(b) Windowed spectrum of ε_2^1, estimates using Gauss method and VP

Conductivity profile

Conductivity profile estimates consistent between

- Q-response inversion, using Q_1, Q_2 and Q_3 estimates
- Variable projection, source parameterized up to SH degree and order 3

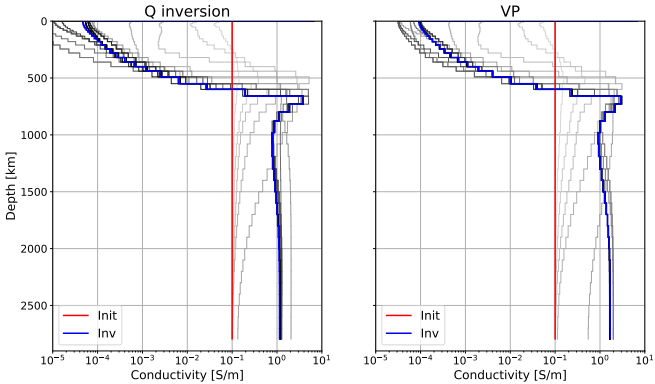

Figure: 1-D conductivity profiles of the mantle obtained from Q-response inversion and VP.

Conductivity estimation: source parameterization

But ... source parameterization has considerable control on the conductivity inversion result

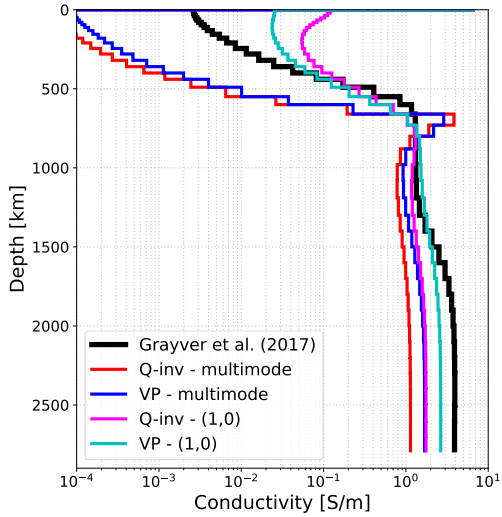

Contents

Comparison between VP variants

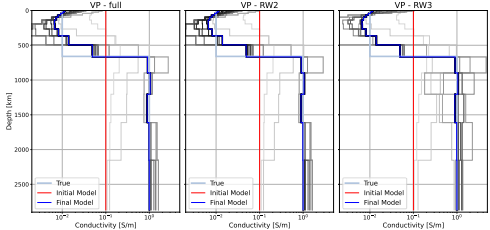

(a) Conductivity profile recovery for VP variants

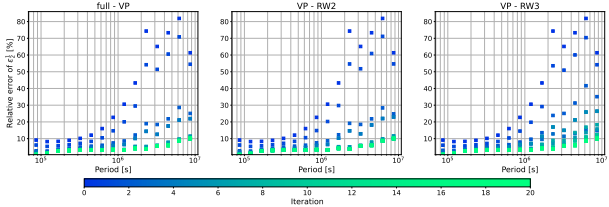

(b) Relative errors for mode ε_2^1

Estimation of Q_1 from real data

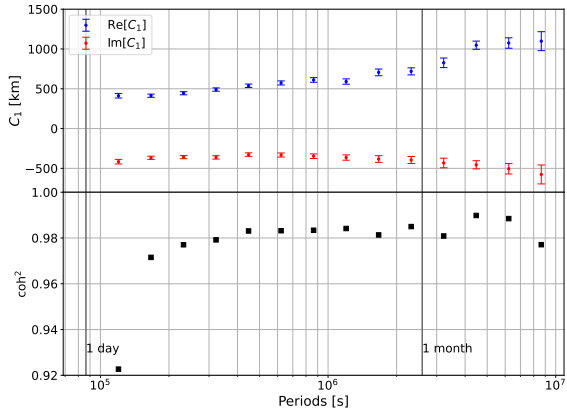

Figure: Q_1 and C_1 responses estimated from mode $(1, 0)$

Coherence between sources estimated from VP and Gauss

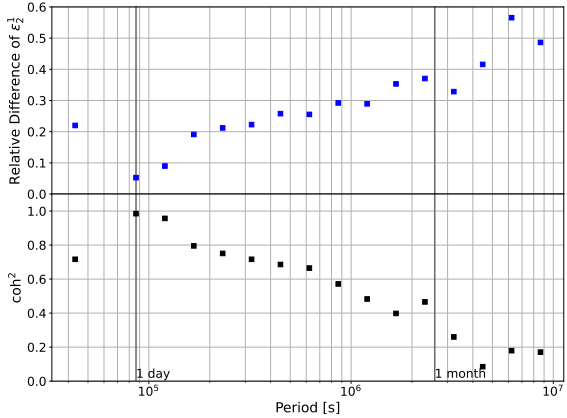

Figure: Relative difference between source estimates from VP and Gauss method, compared with coherence estimated in transfer function regression.